IRRIGATION AND DRAINAGE
Irrig. and Drain. **61**: 240–250 (2012)
Published online 25 October 2011 in Wiley Online Library (wileyonlinelibrary.com) **DOI**: 10.1002/ird.648

EVAPORATION AND WIND DRIFT LOSSES DURING SPRINKLER IRRIGATION INFLUENCED BY DROPLET SIZE DISTRIBUTION†

B. MOLLE[1]*, S. TOMAS[1], M. HENDAWI[2] AND J. GRANIER[1]

[1]*CEMAGREF- UMR-G EAU, Aix en Provence, France*
[2]*Université Aix Marseille II, Marseille, France*

ABSTRACT

Irrigated agriculture is often criticized for its poor resource-use efficiency in the case of sprinkler systems in comparison with localized irrigation. Water losses due to evaporation of droplets during flight and wind drift of droplets out of the target area are often generalized regardless of the context in which they were measured, and may reveal the evaporation capacity of the measurement facility rather than that of the irrigation system itself. Using an approach combining *in situ* measurement (rainfall, electric conductivity) and simulations, losses were estimated according to droplet size distribution. Droplets less than 1 mm in diameter displayed the highest losses. Losses due to evaporation represented 30-50% of total loss; the remaining 50–70% were due to wind causing small droplets to drift outside the target zone. With a Rain Bird 46 sprinkler, total losses for the different periods of the day should not represent more than 20% at any time, or less than 4% for a 24-h irrigation period in the climate conditions that prevail in summer in the south of France. Copyright © 2011 John Wiley & Sons, Ltd.

KEY WORDS: sprinkler irrigation; losses; droplets size; electric conductivity; simulation; measurement

Received 20 September 2010; Revised 9 June 2011; Accepted 9 June 2011

RÉSUMÉ

L'agriculture irriguée est souvent critiquée pour sa faible efficience d'utilisation de l'eau, en particulier dans le cas de l'aspersion en comparaison de l'irrigation localisée. Les pertes d'eau sous forme d'évaporation des gouttes au cours de leur temps de vol et de la dérive des gouttes hors de la zone cible, sont souvent généralisées sans tenir compte de leur contexte de mesure, et peuvent révéler les capacités évaporatives du dispositif de mesure plus que celles du système d'irrigation lui-même. A partir d'une approche combinant des mesures in situ (pluviométrie, conductivité électrique) et des simulations, les pertes ont été estimées en fonction de la distribution de taille des gouttes produites par l'asperseur. La majorité des pertes provient des gouttes plus petites que 1 mm de diamètre. Les pertes par évaporation représentent 30 à 50% des pertes totales, les 50 à 70% restant étant dus à l'influence du vent sur les plus petites gouttes qui dérivent hors de la zone ciblée. En utilisant l'asperseur Rain Bird 46, la perte globale durant les différentes périodes d'une journée d'été dans le sud de la France ne devrait pas dépasser 20% ponctuellement et 4% sur une période d'arrosage de 24 h. Copyright © 2011 John Wiley & Sons, Ltd.

MOTS CLÉS: irrigation par aspersion; pertes; taille des gouttelettes; conductivité électrique; simulation; mesure

INTRODUCTION

Irrigated agriculture is often criticized for its poor resource-use efficiency, which is especially true in the case of sprinkler systems when compared with localized irrigation systems. Water losses through evaporation and wind drift are targets that often relay misconceptions concerning system efficiency due to generalization of figures taken regardless of the context in which they were measured or obtained under uncontrolled conditions.

Water losses during irrigation application (from the nozzle to the soil or crop canopy) can be divided into (i) drift or transport losses: under the influence of wind, smaller drops drift outside the target area, and (ii) evaporation

* Correspondence to: Dr Bruno Molle, Research Engineer, CEMAGREF - UMR-G EAU, RE 3275 Route Cezanne CS 40061 Aix en Provence, 13182 France.
E-mail: bruno.molle@cemagref.fr
†Influence de la distribution de la taille des gouttelettes.sur les pertes par évaporation et la dérive éolienne d'une irrigation par aspersion.

losses: direct evaporation of particles during their flight path from the nozzle to the ground, which can result in complete evaporation of the smallest particles. According to previous studies, these combined losses represent between 2 and 50% of the volume applied in a given period of time (Hermsmeier, 1973; Arshad Ali and Barefoot, 1982) for similar climate conditions. A number of studies have proposed several approaches to estimate these losses through experiments and theoretical analyses.

The experimental approach

Traditionally, water losses during sprinkler irrigation are determined by volumetric measurement of the water collected in collectors placed on the ground (Frost and Schwalen, 1955; Kincaid *et al*., 1986; Kincaid and Longley, 1989; Lorenzini and De Wrachien, 2005). This method of measurement, which is based on the assessment of the quantity of water delivered compared to that collected, gives a global estimation of the losses but does not separate evaporation from drift. Spurgeon *et al*. (1983) found that the losses from a sprinkler irrigation system could reach 30% of the total volume applied, while Steiner *et al*. (1983) measured total losses of around 15%. However, results are often associated with significant errors (Carran, 1976; Playan *et al*., 2005; Hendawi *et al*., 2005) that arise due to inadequate knowledge of the effects of wind on the water collectors. It is therefore important to assess the catching efficiency of the collectors to evaluate the representativity of their measurements and also to quantify losses due to evaporation within the collectors themselves.

To separate losses due to evaporation from those due to drift, Robinson (1973) and McLean *et al*. (2000) measured electric conductivity (EC) of the water in the collectors, and compared these measurements with the EC of water discharged from the sprinkler. The change in EC is directly related to the change in salt concentration, which is a function of evaporation. Using this in the dry conditions of Nebraska, Yazar (1984) found that evaporation represented 1.5–16.8% of the total volume applied by the sprinkler. He concluded that wind and vapour pressure deficit best explained evaporation. Hermsmeier (1973), in California, reported losses of from 0to 50% for short irrigation periods and three to four times more losses (evaporation and drift) during the day than at night.

During irrigation events, a wet microclimate is created that reduces evaporation from the crop canopy (Thompson *et al*., 1986). The actual effect on evaporation is, however, negligible because the free water deposited on the plant evaporates faster than water passing through the plant, thus increasing global consumption (Steiner *et al*., 1983). The suggestion that losses incurred through evaporation and drift during sprinkler irrigation are not real losses (Tarjuelo *et al*., 2000) was questioned by Playan *et al*. (2005) and Martínez-Cob *et al*. (2008) who reported losses (evaporation and drift) of around 9% at night to 16% during the day for a solid set system, and estimated losses to 5% at night and of 9.8% during the day under a moving lateral in Saragossa, Spain. These authors reported that during irrigation, humidity increased by 3.9%, temperature decreased by 0.5 °C, and reference evapotranspiration (ET) (calculated with Penman-Monteith's formula) decreased by $0.023\,\mathrm{mm\,h^{-1}}$. Thus the combined effect only accounts for a 2.1% reduction in ET losses, showing that the losses due to evaporation and drift are in fact real losses with negligible benefit to the crop. Such a conclusion is confirmed by Cavero *et al*. (2009) under sprinkler irrigation, and Tolk *et al*. (1995) under a LEPA system for a corn crop, who observed a 50% reduction of ET during and a few times after irrigation occurred.

Studies by the previously cited authors were based on the use of different sprinklers or sprayers resulting in substantial variability in reported losses even in similar climatic conditions. Different operating parameters and sprinkler configurations result in a wide range of droplet sizes, which strongly influences their flight time and thus their exposure to evaporation. The irrigation setup and the operating conditions define the primary and secondary atomization of the jet spray (Bayvel and Orzechowski, 1993) and thus the size of the droplets. Specifically, the most important factors are nozzle diameter, nozzle geometry and operating pressure (McLean *et al*., 2000; Molle, 2002). It is reasonable to assume that the same determinants of droplet size distribution are also major factors in observed and reported losses.

Applying the theorem of thermodynamics to evaporation losses (thus taking droplet flight time into account), calculated evaporation losses have been shown to represent less than 2% of the total volume applied (Thompson *et al*., 1993).

The analytical approach

The theory related to droplet evaporation phenomena proposed by Ranz and Marshall (1952) can be used to calculate the rate of evaporation of a water particle according to its size (equivalent diameter related to its surface area) and the air vapour pressure deficit. This rate can be used to formulate an equation describing the decrease in diameter of a spherical drop as it evaporates. This equation has been experimentally backed by Goering *et al*. (1972) for droplets diameters around 1 mm.

In the trajectory approach (Crowe *et al*., 1998), the equation describing the droplet trajectory equation is governed by: (i) gravity, (ii) buoyancy force and pressure gradient force, (iii) forces due to water vapour transfer between the droplet and the air, and (iv) friction force. Particle–particle interaction forces are neglected. Edling (1985) proposed a

model that estimates the kinetic energy, the evaporation and the drift of droplets emitted by a low pressure sprinkler. Washington *et al*. (1988) described a more deterministic approach to estimate evaporation from a sprinkler jet and its effects on the microclimate. This approach was inspired by the PSI-Cell (particle-source-in-cell) model developed by Crowe *et al*. (1977) which associates factors that undergo exchange (mass, momentum and thermal energy) between the surrounding air (gaseous phase captured using a Eulerian method) and droplets emitted from the jet (liquid phase determined using a Lagrangian method). The PSI-Cell model does not distinguish between losses due to drift and losses due to evaporation. Thompson *et al*. (1993) designed a model coupling the evaporation of the droplets during flight after being emitted from a sprinkler and evaporation from the ground and/or the crop canopy. The effect of solar radiation was not accounted for during droplet flight, but was included in the energy balance of the soil and crop, while turbulence during droplet flight was no longer taken into account. Recently, more deterministic approaches have been derived from Lagrangian and Eulerian methods. Burger *et al*. (2001) used a 'hybrid procedure' to describe the behaviour of sprayers emitting small numbers of droplets. The dysphasic approach combines an Eulerian approach which converges rapidly for the dispersed and complex sections of the spray, and a Lagrangian approach to account for secondary dispersion. This dual Euler–Lagrange approach has become increasingly popular for modelling particle dispersal and deposition. It is also known as a DPM (discrete phase model).

The above-mentioned studies underline the influence of climatic parameters (wind, vapour pressure deficit, temperature and radiation), but do not explicitly determine the effect of individual parameters and—to a lesser extent – the influence of the characteristics of the jet (diameter, velocity, nozzle shape and dispersal). The following work takes these parameters into account using both experimental and theoretical approaches with the objective of refining the losses measurement method, then analysing the interactions between sprinkler distribution characteristics and the surrounding atmosphere. The numerical approach will help with simulating various climate sequences, to better approach losses over long periods consistent with a sprinkler system operation in real world.

MATERIALS AND METHODS

In the absence of suitable calculation methods water losses during irrigation were assessed by sampling the volumes applied on a grid of collectors. The volumes sampled with the collectors were integrated for each grid area. The resulting sum was then compared with the discharge delivered. The collected volumes were used to measure the variation in water electrical conductivity (EC) as an indicator of local and global evaporation.

Description of the collectors

Collectors in the form of white PVC buckets were used to measure the reconstituted flow rate and change in electrical conductivity. Each bucket collector (diameter 0.25 m, height 0.25 m) was fitted with a funnel designed to minimize contact between the collected water and the atmosphere and the resulting evaporation. The design of the collector also limited the effects of turbulence due to wind. Simulations were conducted to identify the collection rate of different size of droplets generated as a function of wind velocity (Hendawi *et al*., 2005). At a wind velocity of $9\,m\,s^{-1}$, there is only a decrease in the rate of collection of droplets smaller than 1.3 mm in diameter.

Reconstitution of irrigation volume from rainfall measurements

The following investigation was carried out on a plot located on the SupAgro farm in the region of Salon de Provence (south of the Rhone valley, France, Mediterranean climate). The plot is free of obstacles for 500 m in the direction of prevailing winds. The wetted sample area was covered with 400 collectors arranged in a square grid with 2 m spacing (area 40×40 m). An impact sprinkler (Rain Bird 46WH) equipped with two nozzles (2.4 and 4.4 mm in diameter) was placed 0.5 m above the surface of the collectors in the middle of the collector area. The collectors were placed on a layer of sand to facilitate levelling and provide stability. The flow rate was measured at the sprinkler head with an estimated 7error of $\pm 0.5\%$. The sprinkler pressure was measured with a glycerine manometer with an accuracy of $\pm 2.0\%$, and maintained at 350 kPa. Each square of the grid received a volume of water estimated on the basis of the rainfall sampled. The sum of these volumes was compared with sprinkler discharge on the plot.

The radial distribution curve was first measured in the laboratory at CEMAGREF (Aix en Provence, France) on an automated test bench. Only rainfall values above $0.3\,mm\,h^{-1}$ (14.7 g in the collector) were taken into account as established by the ISO 15886–3 standard.

After each test, collectors were weighed with a precision of ± 0.5 g. The entire measuring process took approximately one hour. During this process, as the water in the collectors was subject to evaporation while waiting to be weighed, this was considered as losses and subsequent error. To account for this error, precise volumes of water were measured in groups of five collectors at 10-min intervals to determine losses due to evaporation. The volumes of water used for

this procedure varied from 50 to 500 g (1–10 mm). The resulting estimated evaporation losses (Figure 1) were then used for *a posteriori* correction of the collected rainfall.

On average a 7 g initial evaporation loss could be observed regardless of the collected volume. This initial loss was attributed to droplets deposited on the walls of the collector funnel. These losses remained constant as an absolute value, but increased as a relative value with a decrease in the volume of water collected. After a rapid increase in the percentage of evaporation losses in the first 20 min, the evaporation rate stabilized at 1–3% losses per hour (Table I), in a process which was adjusted using Equation (1):

$$\%\text{Losses} = a \times \left(1 - e^{-b \times \text{time}}\right) \quad (1)$$

Estimation of evaporation through measurement of electrical conductivity

In addition to estimating losses from the reconstruction of sprinkler discharge, evaporation was separated from drift, analysing the variation in electrical conductivity of the water collected at various distances from the sprinkler. Evaporation resulted in a decrease in droplet mass and an increase in the concentration of dissolved salts. Additional collectors located on both main axes of the mesh were used for this purpose. This procedure overestimates losses due to evaporation along the path of droplets in the air because additional evaporation can occur on the walls of the funnel in the collector. Droplets stuck on the funnel can also be leached by others after a short exposure to evaporation.

Electrical conductivity was determined at a reference temperature (20 °C). To calibrate the correction, we placed four samples of the water used in the experiment in the sun, protected from pollution by dust, and measured the decrease in evaporated mass of water (EP%) and the corresponding increase of electrical conductivity (EC%). The regression was linear (Figure 2) following Equation (2):

$$\text{EP}\% = 0.61 * \text{EC}\% \left(\text{Correlation coefficient } R^2 = 0.87\right) \quad (2)$$

To increase the amount of data collected in the field on a grid of collectors, where evaporation may be combined with wind, a series of measurements were conducted later in evaporative conditions (ET0 from 0.7 to 0.95 mm h^{-1}), without wind, using the same sprinkler. The measurements were made at different points along the water distribution radius (every 0.5 m) over periods of 1 h.

Estimation of droplet size distribution

The hydraulic conditions (static pressure, flow rate) defining the initial jet velocity have a major influence on jet disintegration, due to friction with the surrounding air (Kadem, 2005). These factors define the upstream flow conditions that control the distribution of droplet size along the

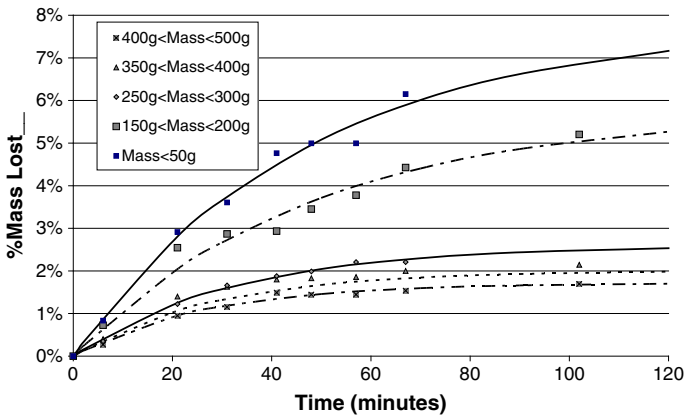

Figure 1. Evaporation losses recorded in sample collectors during the weighing process

Table I. Calculated coefficients for the equation of % losses describing evaporation in collectors during measurement

Class of mass	$M < 50$ g	150 g $< M <$ 200 g	250 g $< M <$ 300 g	400 g $< M <$ 500 g
a	7.78E-02	5.74E-02	2.60E-02	1.72E-02
b	2.12E-02	2.08E-02	3.10E-02	3.78E-02
R^2	0.988	0.972	0.997	0.987

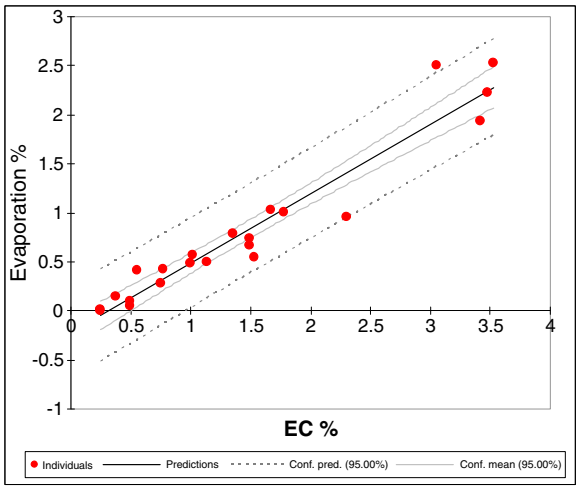

Figure 2. Evolution of electrical conductivity (EC%) of water samples during evaporation. This figure is available in colour online at wileyonlinelibrary.com/journal/ird

jet. The distribution of droplet size generated by the main jet helps explain losses due to evaporation. We measured the distribution of droplet size and velocity along the sprinkler radius using a dual beam spectrometer (DBS) based on the attenuation of infrared beams (Delahaye *et al.*, 2006), installed at ground level. The limit of detection of the DBS is 100 µm; the error on diameters is estimated to be less than 5%. These measurements of droplet size were then used as an input for the simulation of evaporation losses.

The parameters calculated from at least 5000 drop measurements were the average diameter, the median diameter fitted to the numbers (NMD or DN50) and to the volumes (VMD, or DV50), the Sauter diameter (Equation 3) corresponding to the ratio of the sum of volumes to the area of droplets, d being the droplet diameter. The Sauter diameter (D_{32} (m)) characterizes the drag forces, the transfers of mass and heat.

$$D_{32} = \sum^{d^3} \Big/ \sum^{d^2} \tag{3}$$

The distribution of probability of droplet diameters is characterized by the Rosin–Ramler function (1993) as defined in Equation (4), where Y_D (%) is the fraction in mass (or volume) formed by drops with a diameter smaller than D (m), $\bar{d}$(m) corresponds to the value of D where $Y_D = 63\%$, and n is the scatter coefficient of the distribution of probability:

$$Y_D = 1 - e^{-(D/\bar{d})^n} \tag{4}$$

Modelling losses based on droplet size distribution

From the droplet size measurements obtained with the DBS, we calibrated discrete phase model (DPM) describing jet dispersion with the objective of characterizing losses due to evaporation and drift. The DPM is based on a Euler–Lagrange approach applied to a dispersed jet (i.e. volume fraction of liquid < 10%).

The continuous phase (air, index 'g' for gas) is represented by an Eulerian form of Navier–Stokes equations (Equations 5–7):

$$\frac{\partial\left(\alpha_g \rho_g\right)}{\partial t} + \frac{\partial}{\partial x_i}\left(\alpha_g \rho_g U_{g,i}\right) = \dot{m}_{\text{int,g}} \tag{5}$$

$$\frac{\partial\left(\alpha_g \rho_g U_{g,i}\right)}{\partial t} + \frac{\partial}{\partial x_j}\left(\alpha_g \rho_g U_{g,j} U_{g,i}\right) = -\alpha_g \frac{\partial P_g}{\partial x_i} + \mu \frac{\partial^2 U_{g,i}}{\partial x_j \partial x_j} + \alpha_g \rho_g f_g + F_{g,\text{int},i} \tag{6}$$

$$\frac{\partial\left(\alpha_g \rho_g h_g\right)}{\partial t} + \frac{\partial}{\partial x_j}\left(\alpha_g \rho_g U_{g,j} h_g\right) = -\frac{\partial \dot{q}_{g,j}}{\partial x_j} + H_{\text{int,g}} \tag{7}$$

where α_g is the volume fraction of the gaseous phase and ρ_g (kg m^{-3}) is the density. These equations describe respectively the conservation of:

- the mass of vapour in the gaseous mix (Equation 5) with $\dot{m}_{\text{int,g}}$ (kg s^{-1} m^{-3}) as the transfer rate of water per unit of volume to the benefit of the gaseous phase;
- the momentum (Equation 6) with:

- f_i (m^3 s^{-2}): volumetric forces such as gravity in our case;
- (kg s^{-2}) is the force corresponding to the momentum of the mass of liquid transferred to the gaseous phase, M_p (kg) and U_p (m s^{-1}) being the mass and velocity of particles included in a unit of volume;

- the energy (Equation 7) with:

- h_g (J kg^{-1}) is the mass enthalpy of air;
- $H_{\text{int,g}}$ (W m^{-3}) is the transfer of energy (positive from liquid interface to gaseous phase);
- $\dot{q}_g = \lambda_g \frac{\partial T}{\partial x}$(W) is the heat flux λ_g (J m^{-2} K^{-1}) being the thermal conductivity of the gas and T(K) the temperature.

The evolution of the discrete phase (water) is represented by a Lagrangian equation; the 'p' index refers to particle:

$$dm_p^{\frac{p}{dt}} = -\rho_g A_p S_h \frac{D_{i,m}}{D_p} \frac{M_v}{M_{air}} \frac{P_{vs\,g}}{P_g} \left(\frac{T_{\infty\,p}}{T_p} - HR\right) \tag{8}$$

$$\frac{dU_p}{dt} = F_D\left(U_g - U_p\right) + \frac{\rho_p - \rho_g}{\rho_p} g + \frac{\rho_g}{\rho_p} U_p \frac{\partial U_g}{\partial x} - \frac{U_p}{m_p}\frac{dm_p}{dt} \quad (9)$$

$$m_p C_P \frac{dT_p}{dt} = h_{ch} A_p \left(T_\infty - T_p\right) + \frac{dm_p}{dt} l_V + A_p \varepsilon_p \sigma \left(\theta_R^4 - T_p^4\right) \quad (10)$$

where A_p (m²) is the particle surface area, S_h the adimensional Sherwood number, D_p (m) the diameter, D_{im} (m) the molecular diffusivity coefficient, T_p(K) the surface temperature, T_∞(K) the ambient temperature of the air and P_{vs} (kg m^{-1} s^{-2}) the vapour pressure.

These equations describe respectively:

- the mass transfers (Equation 8) expressed according to Fick's law based on the proportionality between fluxes and differences in concentration.
- the path of a particle (Equation 9):
- $F_D(U_g - U_p)$ is the drag force per unit of mass where

$$F_D = \frac{18\mu_g}{\rho_p D_p^2} \frac{C_D R_e}{24},$$

where

$$R_e = \frac{\rho_g \left\| \overrightarrow{U_p} - \overrightarrow{U_g} \right\| D_p}{\mu_g}$$

the Reynolds number (μ_g being the dynamic viscosity) and C_D the drag coefficient (Morsi and Alexander, 1972; Haider and Levenspiel, 1989);

- $\frac{\rho_p - \rho_g}{\rho_p} g$ are the gravity forces and the buoyancy;
- $\frac{\rho_g}{\rho_p} U_p \frac{\partial U_g}{\partial x}$ is the force generated by the pressure gradient in the fluid;
- $-\frac{U_p}{m_p}\frac{dm_p}{dt}$ is the force related to the variation in droplet mass (evaporation);
- the energy transfer (Equation 10) expresses the variation in sensible heat inside the droplet:
- $h_{ch}A_p(T_\infty - T_p)$ is the term of transfer related to thermal convection where h_{ch} is the coefficient of heat transfer (Wm^{-2} K^{-1});
- $\frac{dm_p}{dt} l_V$ is the latent heat transfer and l_v (J kg^{-1}) is the latent heat per unit of mass;
- $A_p \varepsilon_p \sigma \left(\theta_R^4 - T_p^4\right)$ is the radiation term where θ_R (K) is the radiative temperature and ε_p is the particle emissivity.

The coupling between two phases is based on the terms of exchange at the interface and the source/sink terms relative to the mass (Equation 5), in the momentum (Equation 6) and in the quantity of heat (Equation 7). This reciprocal coupling is carried out by alternately solving the equations of the discrete and continuous phases until the balance is reached. From this point on, there is no more change in mass, momentum or heat between the two phases in the calculation cell (Patankar, 1980; Weiss *et al*., 1999; Vasquez and Ivanov, 2000).

RESULTS AND DISCUSSION

Measurement in field and outdoor controlled conditions

Estimation of evaporation losses from EC. Results of analysis of variance of the global evaporation losses calculated from the measurements made in windy conditions (see Table II for the climate conditions observed) which was conducted accounting for the following parameters: vapour pressure deficit (DS, kPa) and wind velocity (V, m s^{-1}), based on data collected at various standard distances (R_{std} = radius/max. radius) from the sprinkler (see Figure 3), showed that each of the parameters had a significant effect and, when taken together, explained at least 60% of variability.

Table II. Synthetic results of measurement of evaporation losses (%EP) and calculated losses due to evaporation and drift losses (%EP and *D*) according to the two different models

Date	Test Init.	Test End	Temp T (°C)	Relative humidity RH (%)	I (W m^{-2})	V (m s^{-1})	VPD (kPa)	ETo (mm h^{-1})	Measured losses (%)	Calculated losses (V, VPD, ETo) (%)	Calculated losses (I, V, VPD) (%)
12/08/03	14:28	15:58	34.4	45	732	2.8	2.97	0.83	11.0	10.7	11.0
11/08/03	14:13	15:43	35.8	30	776	3.5	4.10	0.95	11.6	12.0	12.0
08/08/03	01:07	02:37	22.9	55	2	0.7	1.27	0.03	0.6	0.8	0.5
07/08/03	20:45	22:15	28.7	34	2	1.0	2.60	0.07	3.0	2.9	3.2
06/08/03	11:54	12:54	35.0	28	784	2.2	4.07	0.93	17.9	17.8	17.8
05/08/03	11:00	13:00	35.5	25	780	1.2	4.32	0.90	23.1	23.2	23.2
04/08/03	14:37	16:07	36.8	23	771	3.6	4.79	1.00	13.7	13.6	13.3

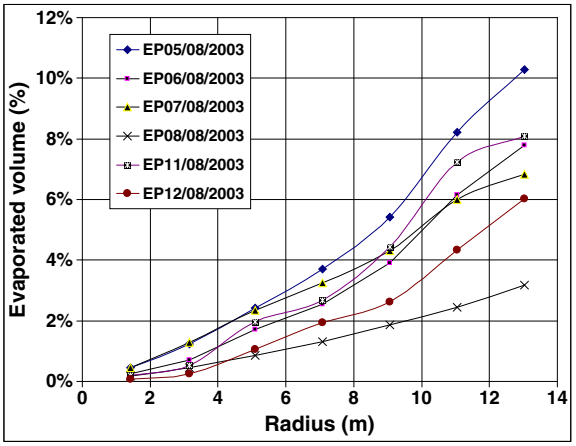

Figure 3. Per cent evaporation losses as a function of distance for field tests. This figure is available in colour online at wileyonlinelibrary.com/journal/ird

Taking radiation or ETo into account did not improve the explanation of these losses because the variability of the situations observed was too small or too big (at night and in the middle of the day) and the number of measurements was insufficient. The main effect was that of the distance. In our climatic conditions, this resulted in a maximum cumulated direct evaporation of 10%, the rest being attributed to drift, which entrained droplets outside the measurement zone. This drift can indirectly benefit the neighbourhood of the target zone. The equation of the losses according to the distance from the sprinkler can be expressed as:

$$\begin{aligned}&\text{Evaporation losses}(\%)\\&\quad = 2.31 + 7.28 * R_{\text{std}} + 2.28 * \text{DS kPa}\\&\quad - 1.078 * V\text{m s}^{-1}(\text{Correlation} = 0.60)\end{aligned} \tag{11}$$

Figure 4 and 5 shows losses as a function of the distance measured in field conditions. The same type of measurements made in no wind conditions, and high evaporative demand was repeated ten times and resulted in lower evaporation losses as a function of distance R_{std} (Figure 4). The order of magnitude was a little higher than 5%. The difference between the two situations (field and no wind outdoor) was attributed to the influence of wind in the evaporation process that may occur during droplet flight as well as during storage on the surface of collectors before falling in the storage part. The main conclusion is that the trends observed in field windy conditions, compared to outdoors with no wind, are similar.

Reconstruction of the flow rate from rainfall distributed on the wetted area

From the initial raw data we weighted the volumes distributed on each point of the grid by its surface area and compared the cumulated volume with the total volume applied through the sprinkler.

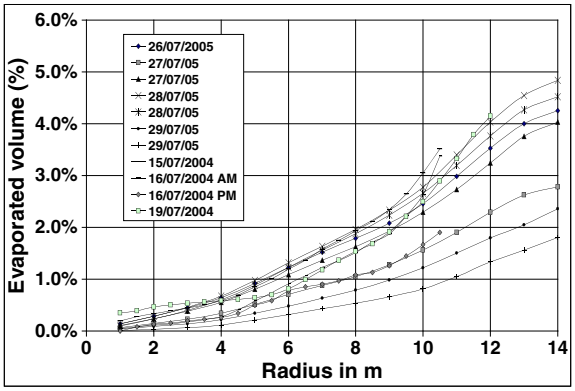

Figure 4. Per cent evaporation losses as a function of distance, tests performed outdoor in controlled conditions (no wind). This figure is available in colour online at wileyonlinelibrary.com/journal/ird

The same principle as for the interpretation of EC was used for the measurements of rainfall according to the standard radius in different directions from the wind. As observed previously, the distance covered by drops or the time of exposure to evaporation was the main factor that explained the total losses.

Results of analysis of variance considering measured total losses (drift + evaporation) as dependent variable, expressed as a percentage of the total volume applied and the climatic parameters measured during *in situ* tests in windy conditions, showed that all the parameters had a highly significant effect, except solar radiation I, probably due to its high variability (0 or 770 W m^{-2}). Restricting the expression to the significant climatic parameters gives

$$\begin{aligned}\%\text{Total losses} = {} & 5.97\text{E}-02 + 2.024\text{E}-02\\&* I\left(\text{W m}^{-2}\right) - 4.626 * V\left(\text{m s}^{-1}\right) + 2.996\\&* \text{DS (kPa)},\ (\text{correlation} = 0.99)\end{aligned} \tag{12}$$

If we use ETo to integrate the radiative component of climate demand (ET), the linear model becomes

$$\begin{aligned}\%\text{Total losses} = {} & 1.3642 - 5.285\\&* \text{V}\left(\text{m s}^{-1}\right) + 2.095\\&* \text{DS (kPa)} + 21.3254\\&* \text{ETo}\left(\text{mm h}^{-1}\right), (\text{correlation} = 0.99)\end{aligned} \tag{13}$$

Several forms of equation were tested: in all cases the wind had the greatest effect followed by radiation and vapour pressure deficit.

Calculation of evaporation losses on a summer day in the south of France

Using Equation (13), we calculated evaporation losses during sprinkler irrigation over a period of two days in the

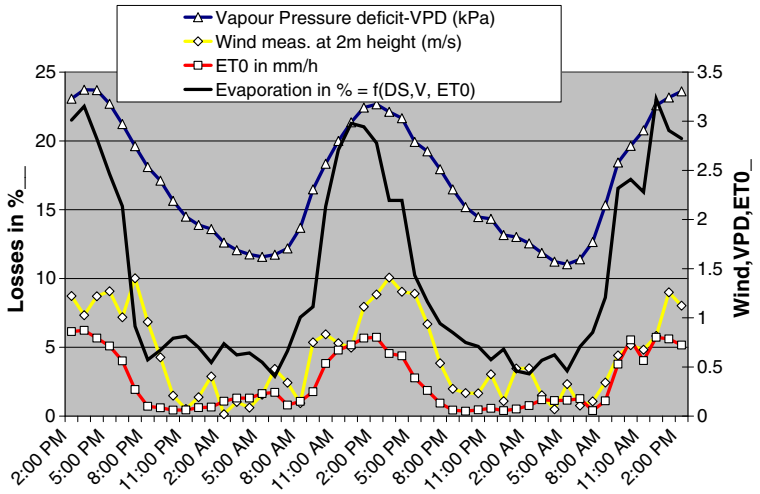

Figure 5. Simulation of evaporation losses on two summer days in 2005 in the south of France. This figure is available in colour online at wileyonlinelibrary.com/journal/ird

summer of 2005, which was particularly hot in the south of France (Figure 5). During this episode temperatures were above 38 °C, but the wind was low for the region. The average losses over a 24-h period were 10.3%, 18.1% for the period from 11 am to 6 pm, and 6.1% from 7 pm to 10 am.

To reduce the risk of losses and to anticipate restricted irrigation in the case of water scarcity, the best period for a ban would be 11 am to 6 pm, which would reduce losses by 6%. If bans are to be established based on meteorological variables, it is recommended to concentrate on wind velocity more than on temperature, since wind velocity has the greatest impact.

Ballistic and thermodynamic simulation

Modelling the ballistics of evaporating drops on their path through the air. First we evaluated the effect of wind velocity on the droplets' path, and then the effects of climatic variables on droplet size distribution.

Initial conditions. The distribution of particles injected into the air was characterized by a Rosin–Ramler distribution comprising 20 classes of diameters that are representative of the droplets measured by the DBS. The Rosin–Ramler distribution parameters are:

$$\bar{d} = 3.65\text{mm}; n = 4.5; D_{\min} = 0.1\text{mm}; D_{\max} = 5.3\text{mm}$$

The velocity of droplets at the injection point was 20 m s^{-1} in the direction of the jet, at an angle of 23° with the horizontal. The initial temperature of the water varied between 20 and 30 °C.

Climatic conditions. To highlight the influence of wind on flight time we performed two simulation series: (i) without wind and (ii) with a wind velocity of $V = 4$ m s^{-1} (maximum velocity recommended for sprinkler irrigation). The direction is identical to that of the jet and parallel to the ground.

This results in the lengthening (downwind) or shortening (upwind) of the flight time of the droplets. The mass fraction of vapour in the air varies from 0.3 to 3.2% corresponding to values of relative humidity, HR, varying from 10 to 70% depending on the temperature. The simulation conditions are summarized in Table III and are referred to in the following paragraphs.

Calculation of the trajectory of the droplets

The flight time of the particles was either the time elapsed between the droplets' exit from the nozzle and their arrival on the ground or exit from the calculation domain. Flight time was slightly affected by the wind, varying between 1.3 and 5.8 s without wind, and 1.2 and 6.1 s with a wind of 4 m s^{-1} respectively for particles bigger than 1 mm and smaller than 0.15 mm. However, in case of high evaporative conditions droplets smaller than 0.15 mm may induce tier total evaporation. Figure 6 plots the distance travelled by the droplets according to the climate conditions presented in Table III with a wind of 4 m s^{-1} and without. Wind applied in the direction of the jet increased the horizontal component of the velocity and slightly decreased the effect of gravity on the droplets. Figure 6 shows that wind increases the distance travelled by a droplet by 4 m for droplets with diameters 0.4 mm. For smaller droplets drift was higher: the maximum radius of throw of such droplets reached 25 m corresponding to an increase of more than 20 m in comparison with no wind.

Table III. List of climate parameters used for the simulations

Case ID	Wind ($m\,s^{-1}$)	Water temp. (°C)	Air temp. (°C)	RH (%)	VPD (kPa)	Th (P, h)	Tr (p, RH)
1029	0	20	30	70	1.27	25.48	24.25
1028	4	20	30	50	2.12	21.94	18.67
1027	0	20	30	50	2.12	21.94	18.67
1009	0	30	40	70	2.21	34.60	34.07
1019	0	20	40	70	2.21	34.60	34.07
1026	4	20	30	40	2.55	19.98	15.10
1025	0	20	30	40	2.55	19.98	15.10
1024	4	20	30	25	3.18	16.75	7.94
1023	0	20	30	25	3.18	16.75	7.94
1007	0	30	40	50	3.69	30.23	28.00
1017	0	20	40	50	3.69	30.23	28.00
1005	0	30	40	40	4.43	27.73	24.14
1015	0	20	40	40	4.43	27.73	24.14
1004	4	30	40	25	5.53	23.46	16.42
1014	4	20	40	25	5.53	23.46	16.42
1003	0	30	40	25	5.53	23.46	16.42
1013	0	20	40	25	5.53	23.46	16.42
1002	4	30	40	10	6.64	18.38	2.68
1012	4	20	40	10	6.64	18.38	2.68
1001	0	30	40	10	6.64	18.38	2.68
1011	0	20	40	10	6.64	18.38	2.68

Droplet evaporation

The objective of this part is to understand how evaporation affects the droplets through its variation of temperature during flight as a function of its diameter (Figure 7). As shown in Figure 7, the smaller droplets are the most sensitive to temperature. The temperature of large particles varies very slightly from their initial injection value of 20 or 30 °C. Apart from the diameter effect, particles can be divided into two groups depending on whether the final temperature of the droplet at the end of flight is lower or higher than at the beginning. When the temperature is lower, water from the droplet has consumed heat to change phase, as will be illustrated in the following paragraph. When the temperature is higher, heat exchanged generally remains as sensible heat without inducing vaporization of the droplets because of a low vapour pressure deficit (configurations 1028, 1009, 1019, 1017 and 1014; Table III) even in the case of smaller particles.

It appears that the main factor influencing direct evaporation is droplet size. Other phenomena should also be taken into account, although they have less effect (e.g. radiation, relative humidity and wind velocity). Taken individually, the effects of radiation and relative humidity on evaporation are low. Radiation induces an increase of up to 10% in evaporation in the case of small droplets and when the relative humidity is high. The wind has a major effect on the evaporation process by increasing the renewal of the air surrounding the flying drops with unsaturated air. The effect of the wind is shown in the two examples in Figure 8 (case 1023, 1024, and 1025, 1026), in which the evaporation rate is represented per unit of time. Wind increases the losses and the travelled distance; its impact decreases as the droplet diameter increases.

Droplet size appears to be the main determining factor in the rate of evaporation. It decreases exponentially with increasing diameters leading to overall losses during flight time of between 3 and 14% per second of flight, in the conditions described in Table III. In highly evaporative conditions, below a diameter of 0.4 mm the droplets mass may fall sharply and losses reach 10 and 70% per second of flight depending on the climatic conditions. Beyond 0.5 mm, the losses are systematically lower than 10%, tending asymptotically towards zero with increasing diameters (see Figure 9). Nevertheless, even if the big droplets lose only a tiny percentage of their mass, it actually corresponds to the highest proportion of losses by evaporation because of the volume they represent (see Figure 10).

These simulations enabled us to clarify the proportion of water that can be evaporated from a set of combinations

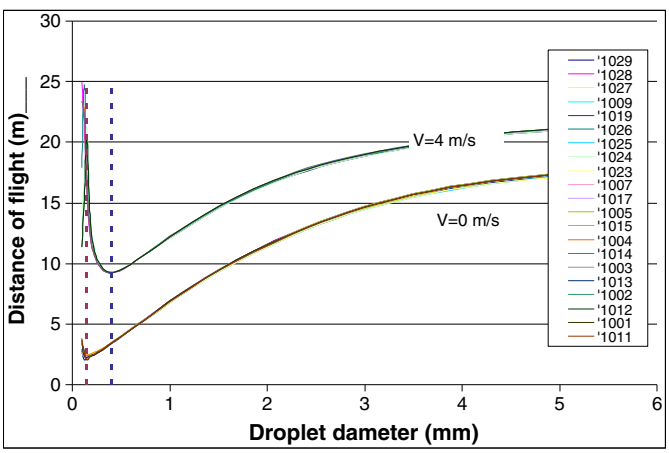

Figure 6. Influence of wind on the distance travelled by the droplet. This figure is available in colour online at wileyonlinelibrary.com/journal/ird

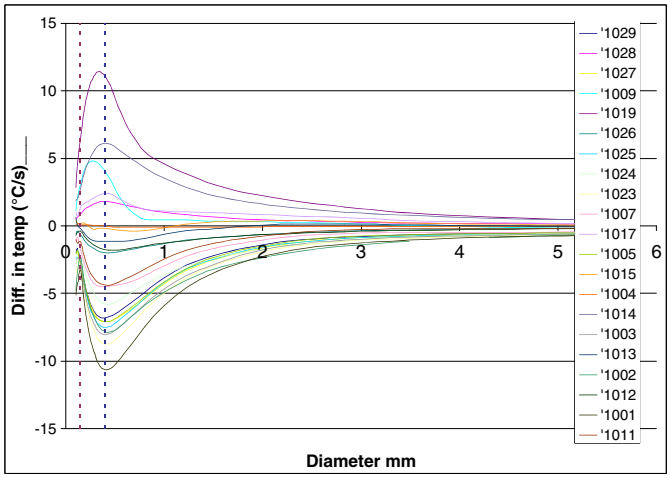

Figure 7. Difference in droplet temperature between injection and the end of flight as a function of droplet diameter. This figure is available in colour online at wileyonlinelibrary.com/journal/ird

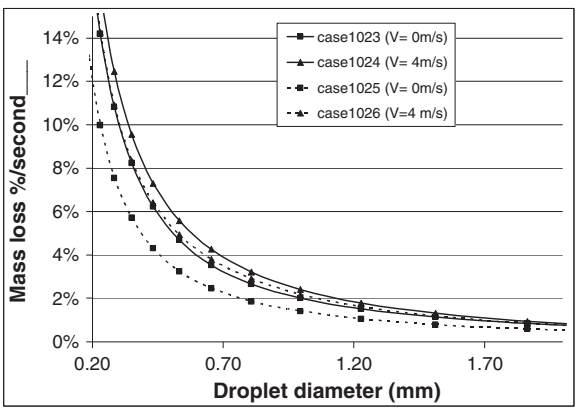

Figure 8. Effect of wind velocity on direct evaporation

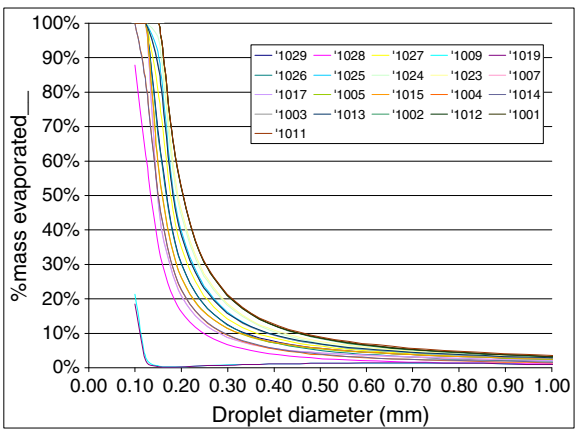

Figure 9. Evaporation of droplets as a percent of their initial mass per second. This figure is available in colour online at wileyonlinelibrary.com/journal/ird

between the droplet size and climatic conditions. At the end of this study it was clear that droplets with a diameter of less than 0.15 mm could be completely lost due to direct evaporation or drift. A wind of 4 m s^{-1} is enough to drag these droplets out of the target area for irrigation.

CONCLUSIONS

We were able to show that the biggest droplets distributed by sprinkler in test are less sensitive to evaporation: their maximum losses of mass during the 2 s their flight lasted did not exceed 2%, for droplets with a diameter greater than 1.5 mm, and 1% for droplets with a diameter greater than 2.5 mm. On the other hand smaller droplets with a low inertia are exposed to evaporation for longer and droplets with a diameter of less than 1 mm can evaporate completely, provided air flow turbulence keeps them in suspension. We worked with low winds experimentally as well as numerically to better understand the process of evaporation itself. However the wind remains the main factor that explains losses by drift. Compared with the data based on EC measurements, we can conclude that approximately 30–50% of the losses were connected to the exposure of particles to the air evaporation potential, which can be increased by radiation. The remaining 50–70% was due to the influence of wind during the flight of the droplets, and in particular on small droplets that drift outside the target zone.

Nevertheless simulated losses remain low with regard to the amounts that were measured. The actual losses estimation may be considerably disturbed by errors of measurement, part of which we detailed in this paper.

Thus, concerning irrigation bans in the case of water scarcity, it is more important to pay attention to wind than to temperature and radiation. Wind alone can explain about two thirds of total losses. As wind and temperature are usually associated, limiting irrigation during the warmest hours of the day is the most sensible solution, but may lead farmers to oversize their irrigation systems so they can irrigate

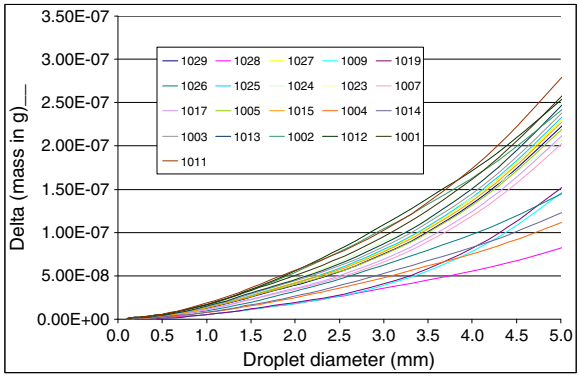

Figure 10. Evaporation losses of mass per unit time according to droplet size. This figure is available in colour online at wileyonlinelibrary.com/journal/ird

faster. If we want to reduce the risk of losses connected with the decline in distribution uniformity, the wind has to be considered prior to evaporation.

REFERENCES

Arshad Ali SM, Barefoot AD. 1982. Low trajectory sprinkler patterns and evaporation. ASAE paper, No. 81–2085; 189–196.

Bayvel ET, Orzechowski Z. 1993. *Liquid Atomization*. Taylor & Francis: UK; 462 pp.

Burger M, Klose G, Rottenkolber G, Schmehl R, Schäfer O, Koch R, Wittig S. 2001. A Combined Eulerian and Lagrangian Method for prediction of Evaporating Sprays. In *Proceedings of DETC'01*. 2001 ASME Design Engineering Technical Conferences: New Orleans, Louisiana, USA.

Carran PS. 1976. A Preliminary Study of the Efficiency of Catch-Cans Used for Irrigation Sprinkler Testing. Internal Report No. 78. New Zealand Agricultural Engineering Institute.

Cavero J, Medina ET, Puig M, Martinez-Cob A. 2009. Sprinkler irrigation changes maize canopy microclimate and crop water status, transpiration, and temperature. *Agronomy Journal* **101**: 854–864.

Crowe CT, Sommerfeld M, Tsuji Y. 1998. *Multiphase Flows with Droplets and Particles*. CRC Press LLC: Boca Raton, Florida 33431; 471 pp. ISBN: 0-8493-9469-4.

Crowe CT, Sharma MP, Stock DE. 1977. The Particle-Source-In Cell (PSI-CELL) model for gas-droplet flows. *Journal of Fluids Engineering* **99**: 325–332. IDS Number: DL132, ISSN: 0098-2202.

Delahaye J-Y, Barthès L, Golé P, Lavergnat J, Vinson JP. 2006. A dual-beam spectropluviometer concept. *Journal of Hydrology* **328**: 110–120. DOI: 10.1016/j.jhydrol.2005.11.048

Edling RJ. 1985. Kinetic energy, evaporation and wind drift of droplets from low pressure irrigation nozzles. *Transactions of ASAE* **28**(2): 511–516.

Georing CE, Bode LE, Gebhardt MR. 1972. Mathematical modeling of a spray droplet deceleration and evaporation. *Transaction de ASAE* **16**(2): 220–225.

Frost KR, Schwalen HC. 1955. Sprinkler evaporation losses. *Agricultural Engineer* **36**(8): 526–528.

Haider A, Levenspiel O. 1989. Drag coefficient and terminal velocity of spherical and nonspherical particles. *Powder Technology* **58**: 63–70. IDS Number: U2698. ISSN: 0032-5910.

Hendawi M, Molle B, Folton C, Granier J. 2005. Measurement accuracy analysis of sprinkler irrigation rainfall in relation to collector shape. *ASCE – Journal of Irrigation and Drainage Engineering* **131**(5): 477–483. DOI: 10.1061/(ASCE)0733-9437(2005)131:5(477).

Hermsmeier, LF. 1973. Evaporation during sprinkler application in a desert climate. ASAE Paper. Vol, 73-216.

Kadem N. 2005. Atomisation du jet d'un canon d'irrigation: modélisation eulérienne et validation. PhD thesis, University of Marseille III; 132 pp.

Kincaid DC, Nabil M, Busch JR. 1986. Spray losses and uniformity with low pressure center pivots. ASAE Paper. No. 86-2091.

Kincaid DC, Longley TS. 1989. A water droplet evaporation and temperature model. *Transactions of ASAE* **32**(2): 457–463. IDS Number: U3564; ISSN: 0001-2351.

Lorenzini G, De Wrachien D. 2005. Performance assessment of sprinkler irrigation systems. A new indicator for spray evaporation losses. *Irrigation and Drainage* **54**(3): 295–305. DOI: 10.1002/ird.171.

Martínez-Cob A, Playán E, Zapata N, Cavero J, Medina ET, Puig M. 2008. Contribution of evapotranspiration reduction during sprinkler irrigation to application efficiency. *ASCE – Journal of Irrigation and Drainage Engineering* **134**(6). DOI: 10.1061/(ASCE)0733-9437(2008)134:6(745).

McLean RK, Sri Ranjan R, Klassen G. 2000. Spray evaporation losses from sprinkler irrigation systems. *Canadian Agricultural Engineering* **42**(1): 15. IDS Number: 312WE; ISSN: 0045-432X.

Molle B. Characterising droplet distribution of an irrigation sprinkler water application. In ICID 53 rd Conference, July 2002, Montreal, Canada.

Morsi SA, Alexander AJ. 1972. An investigation of particle trajectories in two-phase flow systems. *Journal of Fluid Mechanics* **55**(2):193–208.

Patankar SV. 1980. *Numerical Heat Transfer and Fluid Flow*. Hemisphere: Washington, DC.

Playan E, Salvador R, Faci JM, Zapata N, Martinez-Cob A, Sanchez I. 2005. Day and night wind drift and evaporation losses in sprinkler solid-sets and moving laterals. *Agricultural Water Management* **76**(3): 139–159. DOI: 10.1016/j.agwat.2005.01.015.

Ranz WE, Marshall, WR, Jr. 1952. Evaporation from drops, Part I. *Chemical Engineering Progress* **48**(3): 141–146.

Robinson FE. 1973. Increase in conductivity of irrigation water during sprinkling. *Agronomy Journal* **65**(1): 130.

Spurgeon WE, Thompson TL, Gilley JR. 1983. Irrigation management using hourly spray evaporation loss estimates. ASAE Paper No. 83–2591. St Joseph, Mich.

Steiner JL, Kanemasu ET, Clark RN. 1983. Spray losses and partitioning of water under center pivot sprinkler system. *Transactions of the ASCE*: 1128-1134. IDS Number: RN359; ISSN: 0001-2351.

Tarjuelo JM, Ortega JF, Montero J, de Juan JA. 2000. Modelling evaporation and drift losses in irrigation with medium size impact sprinklers under semi-arid conditions. *Agricultural Water Management* **43**(3): 263–284(22). IDS Number: 294VW; ISSN: 0378-3774.

Thompson AL, Gilley JR, Norman JM. 1986. Simulation of sprinkler water droplet evaporation above a plant canopy. *Transactions of the ASAE* **86**-2108.

Thompson AL, Gilley JR, Norman JM. 1993. A sprinkler water droplet evaporation and plant canopy mode II. *Transactions of ASAE* **36**: 735–741.

Tolk JA, Howell TA, Steiner JL, Krieg DR, Schneider AD. 1995. Role of transpiration suppression by evaporation of intercepted water in improving irrigation efficiency. *Irrigation Science* **16**(2): 89–95.

Vasquez SA, Ivanov VA. 2000. A phase coupled method for solving multiphase problems on unstructured meshes. In *Proceedings of ASME FEDSM'00: ASME 2000 Fluids Engineering Division Summer Meeting*. Boston.

Washington L, Silva C, Larry GJ. 1988. Modeling evaporation and microclimate change in sprinkler irrigation. *Transactions of ASAE*.

Weiss JM, Maruszewski JP, Smith WA. 1999. Implicit solution of preconditioned Navier–Stokes equations using algebraic multigrid. *AIAA Journal* **37**(1): 29–36.

Yazar A. 1984. Evaporation and drift losses from sprinkler irrigation systems under various operating conditions. *Agricultural Water Management* **8**: 439–449.